

Origin of low thermal conductivity in In4Se3

Article

Accepted Version

Luu, S. D. N., Supka, A. R., Nguyen, V. H., Vo, D.-V., Hung, N., Wojciechowski, K. T., Fornari, M. and Vaqueiro, P. ORCID: <https://orcid.org/0000-0001-7545-6262> (2020) Origin of low thermal conductivity in In4Se3. *ACS Applied Energy Materials*, 3 (12). pp. 12549-12556. ISSN 2574-0962 doi: 10.1021/acsaem.0c02489 Available at <https://centaur.reading.ac.uk/94436/>

It is advisable to refer to the publisher's version if you intend to cite from the work. See [Guidance on citing](#).

To link to this article DOI: <http://dx.doi.org/10.1021/acsaem.0c02489>

Publisher: ACS Publications

All outputs in CentAUR are protected by Intellectual Property Rights law, including copyright law. Copyright and IPR is retained by the creators or other copyright holders. Terms and conditions for use of this material are defined in the [End User Agreement](#).

www.reading.ac.uk/centaur

CentAUR

Central Archive at the University of Reading

Reading's research outputs online

This document is confidential and is proprietary to the American Chemical Society and its authors. Do not copy or disclose without written permission. If you have received this item in error, notify the sender and delete all copies.

Origin of Low Thermal Conductivity in In4Se3

| | |
|-------------------------------|---|
| Journal: | ACS Applied Energy Materials |
| Manuscript ID | ae-2020-02489q.R1 |
| Manuscript Type: | Article |
| Date Submitted by the Author: | 13-Nov-2020 |
| Complete List of Authors: | Luu, Son D N; Institute of Research and Development, Duy Tan University Supka, Andrew ; Department of Physics and Science of Advanced Materials Program Nguyen, Van Huy ; Key Laboratory of Advanced Materials for Energy and Environmental Applications Vo, Dai-Viet N. ; Center of Excellence for Green Energy and Environmental Nanomaterials (CE@GrEEN) Tuan Hung, Nguyen; Tohoku University , Frontier Research Institute for Interdisciplinary Sciences Wojciechowski, Krzysztof; AGH University of Science and Technology, faculty of Materials Science and Ceramics Fornari, Marco; Central Michigan University, Physics Vaqueiro, Paz; University of Reading, Chemistry |
| | |

SCHOLARONE™
Manuscripts

Origin of Low Thermal Conductivity in In_4Se_3

Son D. N. Luu^{1*}, Andrew R. Supka², Van Huy Nguyen³, Dai-Viet N. Vo⁴, Nguyen T. Hung⁵,
Krzysztof T. Wojciechowski^{6,7}, Marco Fornari², Paz Vaqueiro^{8*}

¹Institute of Research and Development, Duy Tan University, Da Nang, 550000, Viet Nam

²Department of Physics and Science of Advanced Materials Program, Central Michigan
University, Mt. Pleasant, Michigan, 48859 USA

³Key Laboratory of Advanced Materials for Energy and Environmental Applications, Lac Hong
University, Dong Nai 810000, Viet Nam

⁴Center of Excellence for Green Energy and Environmental Nanomaterials (CE@GrEEN),
Nguyen Tat Thanh University, 300A Nguyen Tat Thanh, District 4, Ho Chi Minh City 755414,
Viet Nam

⁵Frontier Research Institute for Interdisciplinary Sciences, Tohoku University, Sendai, 980-
8578, Japan

⁶AGH University of Science and Technology, Faculty of Materials Science and Ceramics,
Thermoelectric Research Laboratory, 30 Mickiewicza, 30-059 Cracow, Poland

⁷ The Lukasiewicz Research Network –, The Institute of Advanced Manufacturing Technology,
Centre of Thermoelectric Materials Research, 37A Wroclawska, 30-011 Cracow, Poland

⁸Department of Chemistry, University of Reading, Whiteknights Park, Reading RG6 6AD,
England, United Kingdom

1
2
3
4
5
6
7
8
9 **Abstract**

10
11
12 In_4Se_3 is an attractive *n*-type thermoelectric material for mid-range waste heat recovery, owing
13 to its low thermal conductivity ($\sim 0.9 \text{ W}\cdot\text{m}^{-1}\cdot\text{K}^{-1}$ at 300 K). Here, we explore the relationship
14
15 between the elastic properties, thermal conductivity and structure of In_4Se_3 . The experimentally-
16
17 determined average sound velocity (2010 m s⁻¹), Young's modulus (47 GPa), and Debye
18
19 temperature (198 K) of In_4Se_3 are rather low, indicating considerable lattice softening. This
20
21 behavior, which is consistent with low thermal conductivity, can be related to the complex
22
23 bonding found in this material, in which strong covalent In-In and In-Se bonds coexist with
24
25 weaker electrostatic interactions. Phonon dispersion calculations show that Einstein-like modes
26
27 occur at $\approx 30 \text{ cm}^{-1}$. These Einstein-like modes can be ascribed to weakly bonded In^+ cations
28
29 located between strongly-bonded $[(\text{In}_3)^{5+}(\text{Se}^{2-})_3]^-$ layers. The Grüneisen parameter for the soft-
30
31 bonded In^+ at the frequencies of the Einstein-like modes is large, indicating a high degree of
32
33 bond anharmonicity and hence increased phonon scattering. The calculated thermal conductivity
34
35 and elastic properties are in good agreement with experimental results.

36
37
38
39
40
41
42
43
44
45
46
47
48
49
50
51
52
53
54
55
56
57
58
59
60

1
2
3
4
5
6
7
8
9
10
11
12
13
14
15
16
17
18
19
20
21
22
23
24
25
26
27
28
29
30
31
32
33
34
35
36
37
38
39
40
41
42
43
44
45
46
47
48
49
50
51
52
53
54
55
56
57
58
59
60

Keywords

Thermoelectric materials, Thermal conductivity, Grüneisen parameter, Lattice softening, Lone pair.

INTRODUCTION

Worldwide concerns with energy supply and sustainability have stimulated considerable research efforts into thermoelectric materials, which enable direct conversion of waste heat into electrical power. The efficiency of thermoelectric energy recovery is related to the dimensionless thermoelectric figure of merit, ZT , which is given by $ZT=S^2\sigma T/(\kappa_L + \kappa_e)$ where S , σ , T , κ_L , and κ_e are the Seebeck coefficient, electrical conductivity, absolute temperature, lattice, and electronic thermal conductivities, respectively¹. To maximize ZT , materials with low thermal conductivity are required. As a consequence of Wiedemann-Franz law, reducing the electronic thermal conductivity, κ_e , would simultaneously lower the electrical conductivity, σ . Therefore, strategies to reduce the thermal conductivity focus on the lattice component (κ_L), which is related to vibrational energy transport. These strategies include the introduction of species with low-energy localized vibrational modes (the phonon-glass electron-crystal (PGEC) approach)^{2,3,4} designing materials with part-crystalline part-liquid states (the phonon-liquid electron-crystal (PLEC) approach)^{4,5,6,7,8}, grain-boundary engineering^{9, 10}, and the introduction of nano-inclusions^{10,11}.

1
2
3 Understanding the origin of the intrinsically low lattice thermal conductivity found in some
4
5

6 thermoelectric materials is critically important to facilitate the discovery of the next generation of
7
8

9 high-performance candidates^{12,16}. Pseudo-layered In_4Se_3 (Figure 1), a mixed-valence
10
11

12 compound that can be formulated as $(\text{In}^+)[(\text{In}_3)^{5+}(\text{Se}^{2-})_3]^-$, is one of the best performing *n*-type
13
14

15 thermoelectric materials for mid-range waste heat recovery^{17,32}. The thermoelectric properties
16
17

18 of In_4Se_3 are highly anisotropic due to its pseudo-layered structure. Single crystals of $\text{In}_4\text{Se}_{3-\delta}$ (δ
19
20

21 = 0.65) exhibit an impressive $\text{ZT} \approx 1.48$ at 705 K in the direction parallel to the layers, but a much
22
23

24 lower ZT , < 0.5, perpendicular to the layers¹⁷. It has been reported that multiple doping is an
25
26

27 effective strategy to produce polycrystalline samples with similarly high values of ZT , as
28
29

30 exemplified by Pb/Sn-co-doped In_4Se_3 ¹⁹ ($\text{ZT} = 1.4$ at 733 K). The outstanding thermoelectric
31
32

33 performance of In_4Se_3 has been attributed to its low thermal conductivity, which is $\sim 0.9 \text{ W}\cdot\text{m}^{-1}\cdot\text{K}^{-1}$
34
35

36 for the undoped polycrystalline material at room temperature^{17,18,19,32}, while in doped and
37
38

39 selenium-deficient samples, values as low as $\sim 0.4 \text{ W}\cdot\text{m}^{-1}\cdot\text{K}^{-1}$ at 723 K can be reached^{30,31}.
40
41

(a)

(b)

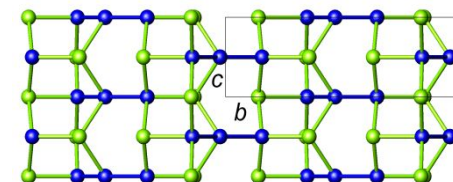
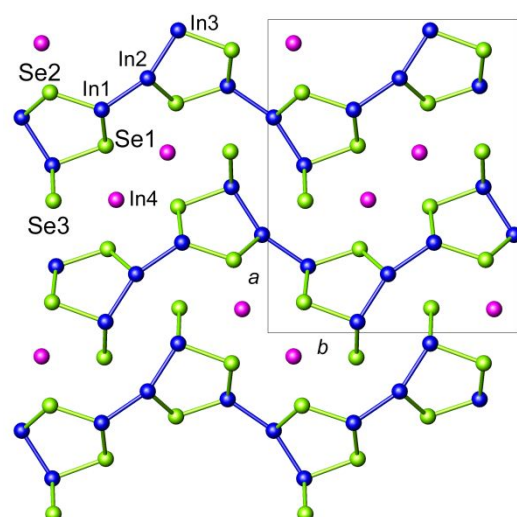


Figure 1. (a) View of the crystal structure of In_4Se_3 along [001]. The In_1 , In_2 , In_3 atoms (dark blue spheres) form $(\text{In}_3)^{5+}$ clusters and are covalently bonded to the selenium atoms (green spheres). The In_4 atoms (dark pink spheres) are located between the $[(\text{In}_3)^{5+}(\text{Se}^{2-})_3]^-$ layers. (b) View of a $[(\text{In}_3)^{5+}(\text{Se}^{2-})_3]^-$ layer along [100]. The unit cell is shown as a grey rectangle.

The low thermal conductivity of selenium-deficient $\text{In}_4\text{Se}_{3-\delta}$ has been proposed that is the result of charge density wave (CDW) induced by a quasi-one-dimensional lattice Peierls distortion¹⁷.

This, however, has been questioned by Osters and co-workers³³, who found that In_4Se_3 behaves as a line phase and does not accommodate selenium deficiency. Instead, selenium-deficient

samples were found to contain indium metal³², while single-crystal X-ray diffraction data provide no evidence of a CDW³³. Moreover, given that stoichiometric In_4Se_3 already exhibits an unusually low thermal conductivity, the investigation of the origin of the low thermal conductivity of this material is essential.

There is a strong link between the elastic properties and the lattice thermal conductivity of a given material³⁴, but little is known about the elastic properties of In_4Se_3 ^{35,36}. Here we describe the correlation between structure and elastic and thermal properties of polycrystalline In_4Se_3 .

With the aid of first-principles calculations, we explore the interplay between bonding, phonon dispersions, and mechanical properties in this material. Our results demonstrate that soft bonding of In^+ ions in the pseudo-layered structure of In_4Se_3 is key to interpret the root of low thermal conductivity in this material.

EXPERIMENTAL

Synthesis and structural characterization

The synthetic procedure for the preparation of In_4Se_3 and the Rietveld refinement using powder X-ray diffraction data were presented in previous work³². Powder X-ray diffraction data

1
2
3 for the powder and the pellet have been included as Supporting Information (SI, Figure S1).
4
5
6

7 Significant bond lengths and angles are included in the SI (Table S1&2). SEM and EDS
8
9

10 measurements are consistent with the nominal composition of In_4Se_3 (SI, Table S3).
11
12

13 ***Property measurements***
14

15 A pellet (density >95%) with a diameter of 10 mm and a thickness of ~ 2.47 mm was used to
16
17

18 measure the longitudinal and transverse acoustic velocities using an ultrasonic instrument
19
20

21 Panametrics Epoch III. Details of this measurement technique are given elsewhere³⁷. These
22
23

24 measured velocities were used to calculate the elastic parameters, and the Poisson ratio³⁸. The
25
26

27 average sound velocity of the sample was calculated from the longitudinal (v_l) and the
28
29

30 measured transverse (v_t) sound velocities using the following expression^{39,40}:
31
32

$$v_a = \left(\frac{1}{3} \left[\frac{1}{v_l^2} + \frac{2}{v_t^2} \right] \right)^{-1/3} \quad (1)$$

33 These values were also used to calculate the Poisson ratio (ν_p) using the following
34
35

36 relationship⁴¹:
37
38

$$\nu_p = \frac{1 - 2 \left(\frac{v_t}{v_l} \right)^2}{2 - 2 \left(\frac{v_t}{v_l} \right)^2} \quad (2)$$

39 The elastic (γ_e) parameter, and Young's modulus (E) were calculated using the equations⁴²:
40
41

$$\gamma_e = \frac{3}{2} \left(\frac{1 + v_p}{2 - 3v_p} \right) \quad (3)$$

$$E = \frac{\rho v_s^2 (3v_t^2 - 4v_p^2)}{(v_t^2 - v_p^2)} \quad (4)$$

where ρ is the density of the material. To estimate the Debye temperature, θ_D , the average sound velocity was used in the expression³⁹:

$$\theta_D = \frac{\hbar}{k_B} \left(\frac{3N}{4\pi V} \right)^{-1/3} v_a \quad (5)$$

where V is the unit-cell volume; N is the number of atoms in a unit cell; k_B is the Boltzmann constant, and \hbar is the Plank constant.

The electrical and thermal conductivities were measured and presented in ref³². The electronic (κ_e) and lattice (κ_{lat}) thermal conductivities were estimated using the electrical conductivity data³² in conjunction with the Wiedemann-Franz law:

$$\kappa_e = L \sigma T \quad (6)$$

where σ is the electrical conductivity and L is the Lorenz number. The value of the Lorenz number⁴³ was estimated using the expression $L = 1.5 + \exp[-|S|/116]$, where L is in $10^{-8} \text{ W } \Omega \text{ K}^{-2}$ and S in $\mu\text{V K}^{-1}$

The minimum lattice thermal conductivity $\kappa_{lat, min}$ of In_4Se_3 was estimated taking into account that⁴⁴:

$$\kappa_{lat} = \frac{1}{3} C_v v_a \Lambda \quad (7)$$

(where C_v and Λ are the volumetric isochoric heat capacity and the phonon mean free path),

by using the interatomic distance as the minimum phonon mean free path. $\kappa_{\text{lat, min}}$ was also

estimated at a high temperature limit using Cahill's model^{14,45}:

$$\kappa_{\text{min}} = \frac{1}{2} \left(\frac{\pi}{6}\right)^{1/3} k_B V^{-2/3} (v_l + 2v_t) \quad (8)$$

First principle calculations

Band structure, density of states, and phonon dispersions were computed using the Quantum

EXPRESSO package⁴⁶ as integrated in AFLOW π ⁴⁷. The Perdew-Burke-Ernzerhof (PBE)

functional was used to describe the exchange-correlation potential. Optimized norm-conserving

PBE pseudopotentials⁴⁸, with a well-converged basis, set corresponding to an energy cut-off of

80 Ry, were used for the wavefunctions. To integrate over the Brillouin zone, a $2 \times 4 \times 8$ (shifted)

grid was used. Electronic transport coefficients were evaluated with PAOFLOW⁴⁹. The finite

difference method using a $1 \times 2 \times 4$ supercell was employed to compute phonons. AFLOW π

uses ElaStic⁵⁰ to determine the nine independent elastic constants, C_{ij} , of orthorhombic crystals

with *Pnnm* space group. The Young modulus and the Poisson ratio were calculated based on

1
2
3 the C_{ij} , by using the Voigt, Reuss, and Hill equations of state. The mode resolved Grüneisen
4
5 parameters were computed within the quasi-harmonic approximation and the lattice thermal
6
7 conductivity was estimated using the Debye-Callaway model⁵¹.
8
9
10
11

12 RESULTS AND DISCUSSION 13 14

15 *Structure and bonding* 16 17

18 In_4Se_3 can be formulated as $(\text{In}^+)[(\text{In}_3)^{5+}(\text{Se}^{2-})_3]^-$, indicating the coexistence of covalent and
19
20 ionic bonding⁵². The crystal structure of In_4Se_3 (Figure 1) contains anionic layers, perpendicular
21
22 to the a-axis, with stoichiometry $[(\text{In}_3)^{5+}(\text{Se}^{2-})_3]^-$. These layers consist of interlocked pentameric
23
24 In_3Se_2 rings, oriented along the c-axis, and linked into bulked layers by linear $(\text{In}_3)^{5+}$ cations.
25
26
27 Within the $(\text{In}_3)^{5+}$ cluster, the distance between In1 and In2 atoms (refer to Figure 1 for atom
28
29 labels) is 2.7239(7) Å while the distance between In2 and In3 is 2.7703(6) Å. These values are
30
31 well below those found in indium metal (3.252 and 3.377 Å)⁵³, and are comparable to the sum
32
33 of the covalent radius for two indium atoms, which is 2.88 Å. Within this layer, the In-Se bond
34
35 distances (SI, Table S1) are also close to the sum of covalent radii for indium (1.44 Å) and
36
37 selenium (1.20 Å)⁵⁴. This indicates that strong covalent bonding occurs within the $[(\text{In}_3)^{5+}(\text{Se}^{2-})_3]^-$
38
39
40
41
42
43
44
45
46
47
48
49
50
51
52
53
54
55
56
57
58
59
60

layers. Assuming tetrahedral coordination for the selenium atoms, Se3 exhibits two In-Se bonds and two dangling bonds (unoccupied coordination sites) whilst Se1 and Se2 possess three In-Se bonds one dangling bond (Figure 1).

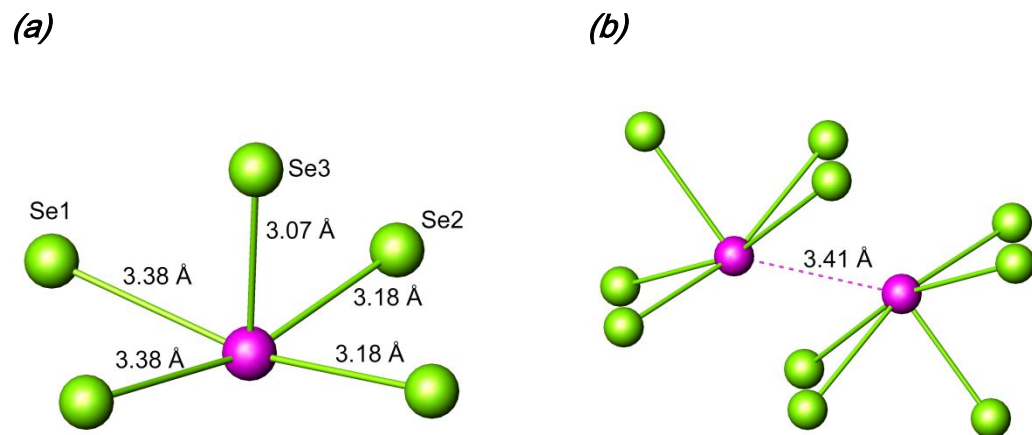


Figure 2. (a) Coordination environment of In4. (b) View of the In4-In4 interaction. Key: In4, dark pink spheres; selenium, green spheres.

Bond valence sums are consistent with a lower oxidation state for In4 (SI, Table S2). This atom, which has a formal oxidation state of In^+ (electronic configuration $[\text{Kr}]5s^2$), is located between the layers. The distance between In4 and the nearest indium atoms within the layers, In1 and In2, are $3.8379(7)$ Å and $3.7530(7)$, respectively, which are considerably larger than those in indium metal. The In4-Se distances are also considerably longer than those within the

[(In₃)⁵⁺(Se²⁻)₃]⁻ layers. In4 adopts distorted square-pyramidal coordination (Figure 2(a)), with In-
Se distances ranging between 3.0688(1) and 3.3802(1) Å (SI, Table S1). These are close to the
sum of ionic radii for In⁺ (1.32 Å)⁵⁵, and Se²⁻ (1.98 Å)⁵⁶. This suggests that In⁺ cations are held
between the layers by electrostatic interactions, while the [(In₃)⁵⁺(Se²⁻)₃]⁻ layers are connected
by strong and directional covalent bonds.

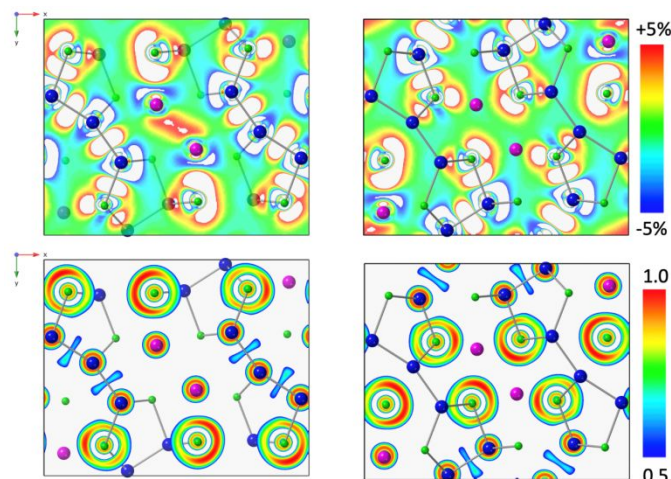


Figure 3. Charge density (top) and ELF (bottom) contour plots in the [001] planes crossing the *c*-axis at fractional coordinates of 0.0 (left) and 0.5 (right). The charge density color scale is centered on the mean value. Meaningful values of the ELF range from 0.5 to close to 1.0. Ions are colored as in Figure 1.

1
2
3 The different nature of the bonding of In_4 is reflected in its considerably larger atomic
4
5 displacement parameter than those for the $(\text{In}_3)^{5+}$ cation found in the covalent layers, evident in
6
7 single-crystal diffraction studies³³. For instance, the atomic displacement parameter for In_4 found
8
9 by Osters and coworkers³³ is 60% larger than those in the $(\text{In}_3)^{5+}$ cation.
10
11
12
13
14
15
16

17 The above considerations are entirely consistent with the results arising from first-principles
18
19 electronic structure calculations. The band structure (SI, Figure S3) is in agreement with
20
21 previously reported results⁵⁷, with the density of states at the top of the valence band dominated
22
23 by Se p and In_4 s states. The presence of anti-bonding states with a substantial degree of cation
24
25 s character at the top of the valence band is a distinctive feature of semiconductors containing
26
27 elements with lone pairs⁵⁸, such as the In^+ cation present in In_4Se_3 . The electrical conductivity
28
29 and the Seebeck coefficients computed as a function of the chemical potential from 300 to 700
30
31 K can be found in the SI (Figure S4).
32
33
34
35
36
37
38
39
40
41
42
43
44
45
46
47
48
49
50
51
52
53
54
55
56
57
58
59
60

1
2
3 these layers, which is evident in these plots. The dangling bonds associated with the selenium
4
5 atoms are also clearly observable, as asymmetrically localized electron clouds. By contrast, the
6
7 nearly spherical ELF around In4 is consistent with ionic bonding. The square-pyramidal
8
9 coordination of In4 would be consistent with the presence of a lone pair of $5s^2$ electrons at the
10
11 missing octahedral vertex. Along the direction of this missing vertex, each In4 atom has a
12
13 neighboring In4 at a distance of 3.4082(3) Å (Figure 2(b)). While this distance is larger than
14
15 those in the $(In_3)^{5+}$ cluster, it is of the same order as those found in In metal. In the valence
16
17 charge plot (Figure 3), there is evidence of charge concentrated between pairs of In4 atoms,
18
19 suggesting that these may be forming dimers.
20
21
22
23
24
25
26
27
28
29
30
31
32

33 *Thermal conductivity*

34
35

36 The heat capacity, thermal diffusivity, and total thermal conductivity of polycrystalline In_4Se_3
37
38 as a function of temperature (Figure 4), previously presented in³², are in good agreement with
39
40 previous reports^{28,29}. The lattice thermal conductivity is the main contributor ($\kappa_{latt} \sim 99.0\%$) to the
41
42 total thermal conductivity of In_4Se_3 (Table 1). The temperature dependence of the thermal
43
44 conductivity computed with the Debye-Callaway model (Figure 4) is in superb coincidence with
45
46
47
48
49
50
51
52
53
54

the experimental values. By using the interatomic distance as the phonon mean free path ($\Lambda \sim 3.2 \text{ \AA}$), we estimated that $\kappa_{lat,min}$ for In_4Se_3 is $\sim 0.3 \text{ W}\cdot\text{m}^{-1}\cdot\text{K}^{-1}$ at room temperature, while with Cahill's model, a value of $\kappa_{lat,min}$ of $\sim 0.4 \text{ W}\cdot\text{m}^{-1}\cdot\text{K}^{-1}$ is found. Our experimental value of κ_{lat} is $\sim 0.84 \text{ W}\cdot\text{m}^{-1}\cdot\text{K}^{-1}$ at 323 K (Table 1), indicating that Λ of In_4Se_3 is larger than the interatomic distance. Therefore, there is still potential for further reductions in thermal conductivity. Indeed, the incorporation of nano-inclusions in In_4Se_3 ²⁷ leads to values of thermal conductivity close to its minimum value.

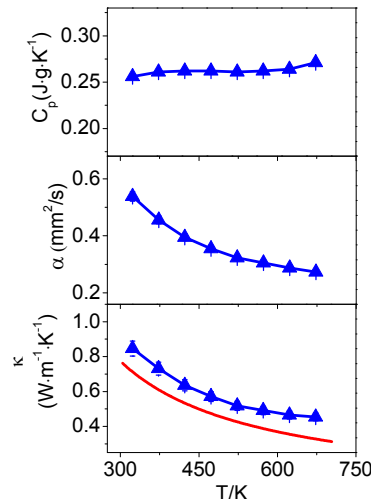


Figure 4. The specific heat, thermal diffusivity, and thermal conductivity of In_4Se_3 as a function of temperature (blue triangles). The temperature dependence of the thermal conductivity

1
2
3 computed with the Debye-Callaway model using parameters from the first-principles is shown
4
5
6 as a red line.
7
8
9
10
11
12
13
14
15

16
17
18 **Table 1.** The electrical conductivity (σ), electronic thermal (κ_e), lattice thermal (κ_{latt}), and total
19 thermal (κ_{tot}) conductivities at 323 K.
20
21
22
23
24
25
26
27
28
29

| | σ (S/m) | κ_e (W \cdot m $^{-1}$ \cdot K $^{-1}$) | κ_{latt} (W \cdot m $^{-1}$ \cdot K $^{-1}$) | κ_{tot} (W \cdot m $^{-1}$ \cdot K $^{-1}$) |
|---------------------------------|----------------|---|---|--|
| ln ₄ Se ₃ | 1965 | 0.01 | 0.84 | 0.85 |

Elastic properties

30 The nine elastic constants calculated by us are consistent with the experimental results
31
32 reported in the literature (Table 2). The elastic properties for ln₄Se₃ determined experimentally
33
34 and through our first-principles calculations are summarized in Table 3. The experimentally-
35
36 determined sound velocities for ln₄Se₃, which in the Debye model would correspond to the group
37
38 velocities of the heat-carrying acoustic phonons, are rather low. These velocities are reasonably
39
40 consistent with the calculated values of the transverse sound velocities, 1381 and 1650 m s $^{-1}$,
41
42
43 and the longitudinal sound velocity, 2870 m s $^{-1}$. Given that it has been shown that κ_{latt} is directly
44
45
46
47
48
49
50
51
52
53
54
55
56
57
58
59
60

1
2
3 proportional to the cube of the average sound velocity⁵⁹, a low sound velocity will result in a low
4
5 thermal conductivity. The Young's modulus of In_4Se_3 ($E \sim 47$ GPa), which is related to its
6
7 stiffness (i.e. its chemical bond strength), is also low. For instance, the Young's modulus of
8
9 In_4Se_3 is significantly lower than those of established thermoelectric materials such as
10
11 $\text{Si}_{0.8}\text{Ge}_{0.2}$ ⁶⁰ ($E \sim 143$ GPa) and Mg_2Si ⁶¹ ($E \sim 117$ GPa), and comparable to other state-of-the art
12
13 thermoelectric materials, including SnSe ³⁷ ($E \sim 28\text{-}40$ GPa), PbSe ³⁷ ($E \sim 62\text{-}65$ GPa), PbTe ^{37, 62}
14
15 ($E \sim 54\text{-}57$ GPa), Cu_2Se ⁶³ ($E \sim 65\text{-}68$ GPa) or those of glass and porous materials, such as
16
17 borosilicate glass ($E \sim 61\text{-}64$ GPa), brick ($E \sim 10\text{-}50$ GPa) and concrete ($E \sim 25\text{-}38$ GPa)⁶⁴.
18
19
20
21
22
23
24
25
26
27
28
29
30
31
32
33
34
35
36
37
38
39
40
41
42
43
44
45
46
47
48
49
50
51
52
53
54
55
56
57
58
59
60

Table 2. Elastic constants for In_4Se_3 in GPa. The experimental data are from ref.³⁶

| | C_{11} | C_{22} | C_{33} | C_{44} | C_{55} | C_{66} | C_{12} | C_{13} | C_{23} |
|--------------|----------|----------|----------|----------|----------|----------|----------|----------|----------|
| This study | 37.6 | 66.7 | 56.7 | 13.7 | 23.7 | 19.9 | 17.9 | 28.0 | 15.4 |
| Experimental | 38.2 | 66.5 | 64.3 | 16.6 | 26.6 | 19.0 | 10.8 | 30.4 | 22.4 |

Materials with weak interatomic bonding usually possess low stiffness and Young's modulus. They are regarded as "softly" bonded materials that result in flattened phonon dispersion curves, and therefore, low sound velocities and low thermal conductivities⁶⁵. Theoretically, the value of

1
2
3 Young's modulus is computed assuming a specific equation of state (EoS), and the calculated
4
5 values using the Voigt, Reuss, and Hill EoS are consistent with the experimental results (Table
6
7 3). For the three EoS, the calculated Poisson ratios (Table 3) are also in excellent agreement
8
9 with the experimental values. The Debye temperature (θ_D) of In_4Se_3 , which is related to the
10
11 maximum phonon frequency ($\omega_D = \frac{k_B}{\hbar} \theta_D$), is low, ~ 198 K. This is also consistent with the low
12
13 thermal conductivity this material exhibits. The phonon dispersion curves for In_4Se_3 computed
14
15 from first principles are presented in Figure 5. The absence of negative branches in the
16
17 vibrational spectrum indicates that the structure is thermodynamically stable. Therefore, a
18
19 distortion leading to a superstructure is not expected for stoichiometric In_4Se_3 . This is entirely
20
21 consistent with the structural study of Osters and coworkers³³, who found no evidence of a
22
23 Peierls-distortion or a CDW in stoichiometric In_4Se_3 . It is also noticeable that the frequency of
24
25 the acoustic modes is very low, suggesting that the bonding is soft with a substantial number of
26
27 low-frequency optical modes, close in energy to the acoustic modes. Although, *per se*, the
28
29 vibrational spectrum is not sufficient to determine thermal transport quantities, the small energy
30
31 difference between optical and acoustic modes suggests that the low-frequency optical phonon
32
33
34
35
36
37
38
39
40
41
42
43
44
45
46
47
48
49
50
51
52
53
54
55
56
57
58
59
60

1 modes will interact strongly with the heat-carrying acoustic phonons, and may therefore be
2
3 interpretative for the low thermal conductivity. By projecting the phonon density of states onto
4
5 each atom, we find that the main contributors to low-frequency modes are the indium atoms,
6
7 and in particular In4. This is consistent with the weak bonding we found for this atom in our
8
9 structural analysis. Visualisations of the atom displacements for selected low-energy optical
10
11 modes, together with the vibrational DOS resolved along different directions in the crystal
12
13 structure, have been included as SI (Figure S5-S9). These indicate that the In4 atoms move
14
15 mainly in the *ab* plane. The large contribution of In4 to the eigendisplacement of the modes at
16
17 low frequency is indicative of Einstein-like vibrations reminiscent of rattling. It is widely
18
19 recognized that localized rattler modes within the acoustic range reduce the lattice thermal
20
21 conductivity, either by resonant scattering or by a reduction in group velocity⁶⁶. Given that our
22
23 analysis of the bonding suggests the presence of In4 dimers, these rattling vibrations might
24
25 involve pairs of In4 atoms.

Table 3. Experimentally and computationally determined elastic properties of In_4Se_3 .

| Polycrystalline In_4Se_3 | Sound velocity (m/s) | | | Derived parameters | | |
|---|-------------------------|-------------------|---------|---|--|----------------|
| | ν_l | ν_t | ν_a | Poisson ratio (ν_p) | Young's modulus E (GPa) | θ_D (K) |
| Experimental | 3150 | 1810 | 2010 | 0.25 | 47 | 198 |
| Computational | 2870 | 1516 ^a | 1695 | 0.26 ^b 0.28 ^c 0.27 ^d | 45.58 ^b 36.56 ^c 42.59 ^d | |

^a Average transverse velocity; ^b Voigt equation of state; ^c Reuss equation of state; ^d Hill equation of state

Anharmonic Effects

First-principles calculations within the quasi-harmonic approximation can be exploited to determine the mode-resolved Grüneisen parameter, which provides a direct measure of the

1
2
3 anharmonicity of bonds (Figure 6(a)). We have demonstrated in the past^{67,68,69} that the presence
4
5 of low-frequency anharmonic modes is a good descriptor for low thermal conductivity.
6
7 Anharmonicity increases phonon-phonon scattering and therefore reduces the lattice thermal
8
9 conductivity. As evidenced by Figure 6(a), the mode-resolved Grüneisen parameter for In_4Se_3
10
11 is considerably larger for In atoms than for Se atoms. Moreover, the largest values of the
12
13 Grüneisen parameter are found for In_4 between 20 and 50 cm^{-1} . In the atom-projected vibrational
14
15 density of states (Figure 5), this frequency range corresponds to the region where the Einstein-
16
17 like dispersion is observed. This is consistent with the weak bonding of In_4 resulting in rattling-
18
19 like vibrations. Calculations of the total energy response to the in-plane displacement of In_4
20
21 (Figure 6(b)) indicate that the total energy is minimally affected by displacements, and therefore
22
23 confirm that the bonding of this atom is soft. It has been shown that anharmonicity can be
24
25 amplified by lone-pair polarization⁷⁰, which could be a contributive factor to the origin of the low
26
27 thermal conductivity of In_4Se_3 , owing to the presence of a lone $5s^2$ pair in In_4 . Our structural
28
29 analysis suggests that the In_4 atoms, which exhibit a highly asymmetric bonding environment,
30
31 might be forming weakly-interacting dimers (Figure 2). We conjecture that, during thermal
32
33

vibrations, the interaction of the lone pairs along the $\text{In}_4\ldots\text{In}_4$ direction will lead to high anharmonicity.

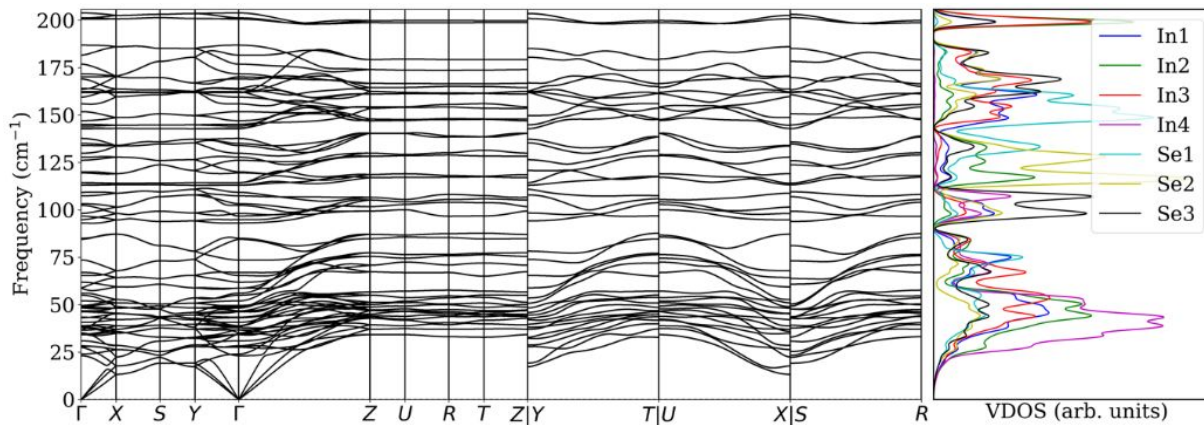


Figure 5. The computed phonons dispersion curves (left) for In_4Se_3 from first-principles and atom-projected vibrational density of states (right). LO-TO splitting is very small.

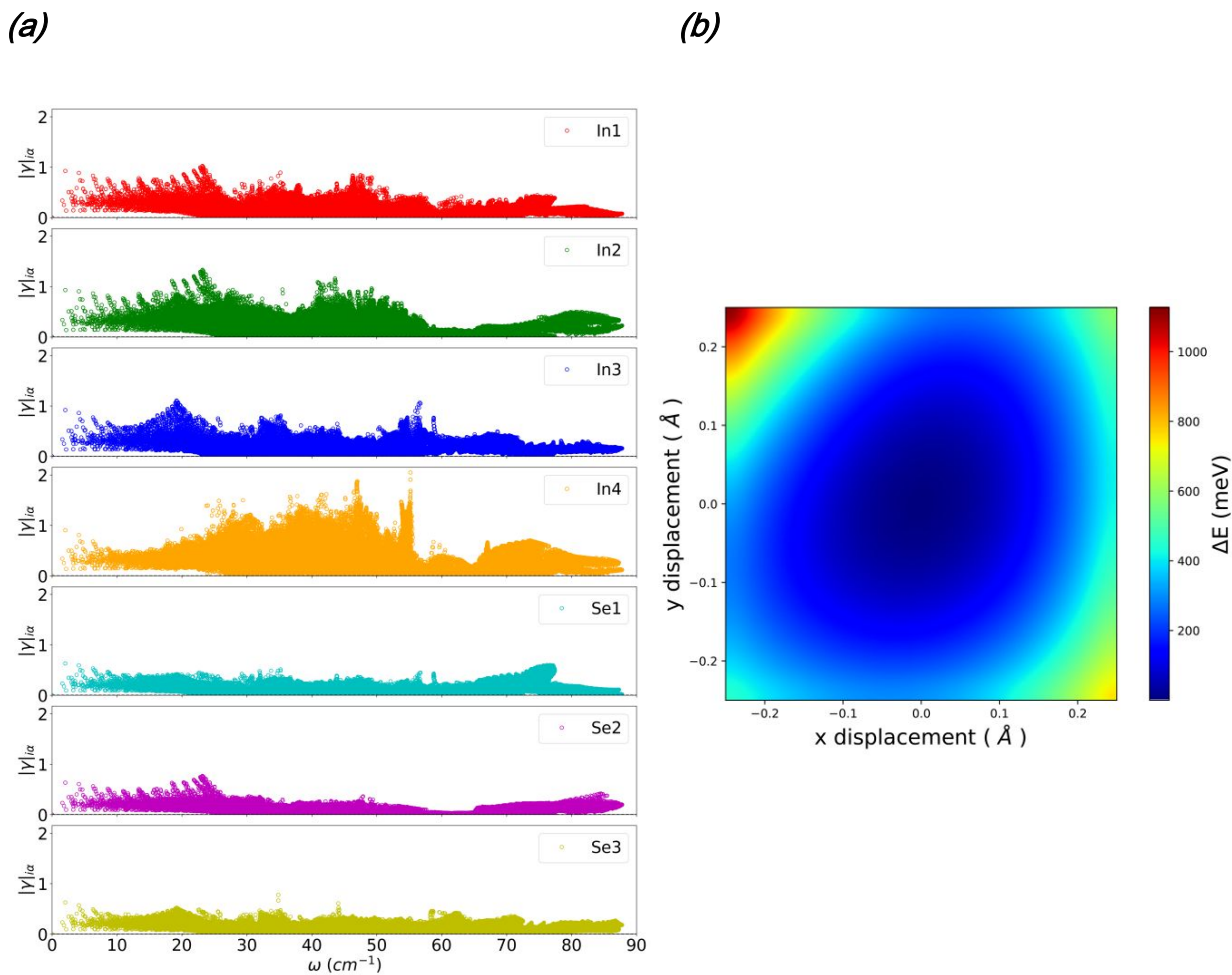


Figure 6. (a) Mode resolved Grüneisen parameters projected on individual atoms. (b) Total energy differences for the symmetrized displacement of the In4 atom along the [001] direction and in the plane x-y.

CONCLUSIONS

Our experimental and computational results demonstrate that, contrary to a previous suggestion which related low thermal conductivity to a Peierls distortion¹⁷, the intrinsically low thermal conductivity of In_4Se_3 is a consequence of the soft bonding of In^+ ions located between covalently-bonded $[(\text{In}_3)^{5+}(\text{Se}^{2-})_3]^-$ layers. This conclusion is strongly supported by the presence of Einstein-like modes in the vibrational density of states, which we attribute to “rattling” vibrations of the weakly-bonded In^+ cations. The synergistic effect of soft bonding and the lone $5s^2$ pair of the In^+ cations leads to a high degree of anharmonicity, as evidenced by large mode-resolved Grüneisen parameters, and hence to more effective phonon scattering.

ACKNOWLEDGMENTS

S. D. N. L and K.T.W thank the Institute of Advanced Manufacturing Technology for hosting and financial support within the TEAM –TECH0076 project of the Foundation for Polish Science, entitled “New approach for the development of efficient materials for direct conversion of heat into electricity project”, co-financed by the European Union under the European Regional Development Fund. P.V. acknowledges The Leverhulme Trust for Research Project Grant

1
2
3 (RPG-2019-288). A.R.S. and M.F. thank the Institute for Cyber-Enabled Research at Michigan
4
5
6 State University for access to computational facilities, and Giovanni Pizzi at materialscloud.org
7
8
9
10 for technical support.
11
12
13
14

15 Supporting Information 16 17 18

19 The following files are available free of charge:
20
21
22

23 Tables of bond lengths and angles, bond valence sums, powder XRD of powdered and pellet
24
25 samples, SEM and EDS data, the calculated electronic structure, calculated Seebeck and
26
27 electrical conductivity, the visualisations of the atom displacements, and vibrational DOS data
28
29
30 (PDF).
31
32
33
34
35
36
37

38 AUTHOR INFORMATION 39

40 Corresponding Author 41

42 *E-mail: iuudngocson@duytan.edu.vn; p.vaqueiro@reading.ac.uk
43
44

49 Author Contribution 50

51 The manuscript was written through the contributions of all authors.
52
53

Notes

The authors declare that they have no known competing financial interests or personal relationships that could have appeared to influence the work reported in this paper.

1
2
3 **REFERENCES**
4
5
6

7 (1) Rowe, D. M., *Thermoelectrics Handbook: Macro to Nano*, ed. D. M. Rowe, CRC Press,
8
9 Taylor and Francis, Boca Raton, 2006, 1.

10
11
12
13
14 (2) Slack, G. A., New materials and performance limits for thermoelectric cooling. In *CRC*
15
16
17
18 *Handbook of Thermoelectrics*; Rowe. D.M., Ed.; CRC, Boca Raton, 1995, **34**, 407-440.

19
20
21
22 (3) Yin, Y., Baskaran, K., Tiwari, A., A Review of Strategies for Developing Promising
23
24
25 Thermoelectric Materials by Controlling Thermal Conduction, *Phys. Status Solidi A*, 2019,

26
27
28
29 1800904
30
31

32
33 (4) Yang, J., Wang, Y., Yang, H., Tang, W., Yang, J., Chen, L., Zhang, W., Thermal transport
34
35 in thermoelectric materials with chemical bond hierarchy, *J. Phys.: Condens. Matter*, 2019, **31**,

36
37
38
39 183002
40
41

42
43 (5) Liu, H., Shi, X., Xu, F., Zhang, L., Zhang, W., Chen, L., Li, Q., Uher, C., Day, T., Snyder,
44
45
46 G.J., Copper ion liquid-like thermoelectrics, *Nat. Mater.*, 2012, **11**, 422-425.

1
2
3
4
5 (6) Qiu, W., Xi, L., Wei, P., Ke, X., Yang, J., Zhang, W., Part-crystalline part-liquid state and
6
7
8 rattling-like thermal damping in materials with chemical-bond hierarchy, *Proc. Natl. Acad. Sci.*
9
10
11 USA 2014, 111, 15031
12
13
14
15
16 (7) Li, D., Zhao, H., Li, Sh., Wei, B., Shuai, J., Shi, Ch., Xi, X., Sun, P., Meng, Sh., Gu, L., Ren,
17
18
19 Zh., Chen, X., Atomic Disorders Induced by Silver and Magnesium Ion Migrations Favor High
20
21
22 Thermoelectric Performance in α -MgAgSb Based Materials, *Adv. Funct. Mater.* 2015, 25, 6478–
23
24
25
26 6488
27
28
29
30 (8) Zhao, K., Qiu, P., Shi, X., Chen, L., Recent Advances in Liquid-Like Thermoelectric Materials,
31
32
33 *Adv. Funct. Mater.* 2019, 1903867
34
35
36 (9) Kim, S.II., Lee, K.H., Mun, H.A., Kim, H.S., Hwang, S.W., Roh, J.W., Yang, D.J., Shin,
37
38
39 W.H., Li, X.S, Lee, Y.H., Snyder, G.J., Kim, S., Dense dislocation arrays embedded in grain
40
41
42 boundaries for high-performance bulk thermoelectrics, *Science*, 2015, **348**, 109–114.
43
44
45
46
47
48 (10) Kim, W., Strategies for engineering phonon transport in thermoelectrics, *J. Mater. Chem.*
49
50
51 C, 2015, **3**, 10336–10348
52
53
54
55
56
57
58
59
60

1
2
3
4
5 (11) Kanatzidis, M. G., Nanostructured thermoelectrics: The New Paradigm? *Chem. Mater.*,
6
7
8 2010, **22**, 648-659.
9
10
11
12

13 (12) Samanta, M., Pal, K., Pal, P., Waghmare, U. V., Biswas, K., Localized Vibrations of Bi
14
15 Bilayer Leading to Ultralow Lattice Thermal Conductivity and High Thermoelectric Performance
16
17
18 in Weak Topological Insulator n-Type BiSe, *J. Am. Chem. Soc.* 2018, **140**, 17, 5866–5872.
19
20
21
22
23

24 (13) Acharyya, P., Ghosh, T., Pal, K., Kundu, K., Rana, K. S., Pandey, J., Soni, A., Waghmare,
25
26 U. V., Biswas, K., Intrinsically Ultralow Thermal Conductivity in Ruddlesden–Popper 2D
27
28 Perovskite $\text{Cs}_2\text{PbI}_2\text{Cl}_2$: Localized Anharmonic Vibrations and Dynamic Octahedral Distortions,
29
30
31 *J. Am. Chem. Soc.* 2020, **142**, 36, 15595–15603.
32
33
34
35
36
37
38

39 (14) Sarkar, D., Ghosh, T., Roychowdhury, S., Arora, R., Sajan, S., Sheet, G., Waghmare, U.
40
41 V., Biswas, K., Ferroelectric Instability Induced Ultralow Thermal Conductivity and High
42
43 Thermoelectric Performance in Rhombohedral p-Type GeSe Crystal, *J. Am. Chem. Soc.* 2020,
44
45
46 142, 28, 12237–12244.
47
48
49
50
51
52
53
54
55
56
57
58
59
60

1
2
3
4
5 (15) Dutta, M., Matteppanavar, S., Prasad, M. V. D., Pandey, J., Warankar, A., Mandal, P.,
6
7
8
9 Soni, A., Waghmare, U. V., Biswas, K., Ultralow Thermal Conductivity in Chain-like TiSe Due to
10
11 Inherent Ti⁺ Rattling, *J. Am. Chem. Soc.* 2019, **141**, 51, 20293–20299.
12
13
14
15
16 (16) Rathore, E., Juneja, R., Culver, S. P., Minafra, N., Singh, A. K., Zeier, W. G., Biswas, K.,
17
18
19 Origin of Ultralow Thermal Conductivity in n-Type Cubic Bulk AgBiS₂: Soft Ag Vibrations and
20
21
22 Local Structural Distortion Induced by the Bi 6s² Lone Pair, *Chem. Mater.* 2019, **31**, 6, 2106–
23
24
25
26
27 2113.
28
29
30
31 (17) Rhyee, J. S., Lee, K.H., Lee, S. M., Cho, E., Kim, S. I., Lee, E., Kwon, Y. S., Shim, J. H.,
32
33
34 Kotliar, G., Peierls distortion as a route to high thermoelectric performance in In₄Se_{3-δ} crystals,
35
36
37 *Nature*, 2009, **459**, 965.
38
39
40
41
42 (18) Rhyee, J. S., Ahn, K., K.H., Lee, Ji, H. S., Shim, J.H., Enhancement of the Thermoelectric
43
44
45 Figure-of-Merit in a Wide Temperature Range in In₄Se_{3-x}Cl_{0.03} Bulk Crystals, *Adv. Mater.*, 2011,
46
47
48
49
50 23, 2191.
51
52
53
54
55
56
57
58
59
60

1
2
3
4
5 (19) Lin, Z. S., Chen, L., Wang, L. M., Zhao, J. T., Wu, L. M., A Promising Mid-Temperature
6
7
8

9 Thermoelectric Material Candidate: Pb/Sn-Codoped $\text{In}_4\text{Pb}_x\text{Sn}_y\text{Se}_3$ *Adv. Mater.*, 2013, **25**, 4800
10
11 – 4806.
12
13
14
15

16 (20) Han, G., Chen, Z-G., Drennan, J., Zou, J., Indium Selenides: Structural Characteristics,
17
18
19 Synthesis and Their Thermoelectric Performances, *Small*, 2014, **14**, 10, 2747-2765.
20
21
22
23

24 (21) Yin, X., Liu, J-Y., Chen, L., Wu, L-M., High Thermoelectric Performance of In_4Se_3 -Based
25
26
27 Materials and the Influencing Factors, *Acc. Chem. Res.*, 2018, **51**, 2, 240-247.
28
29
30
31

32 (22) Ahn, K., Cho, E., Rhyee, J. S., Kim , S. II., Lee , S. M., Lee , K. H., Effect of cationic
33
34
35 substitution on the thermoelectric properties of $\text{In}_{4-x}\text{M}_x\text{Se}_{2.95}$ compounds (M=Na, Ca, Zn, Ga,
36
37
38 Sn, Pb; x=0.1), *Appl. Phys. Lett.*, 2011, **99**, 102110.
39
40
41
42

43 (23) Li, G., Yang, J. Y., Luo, Y. B., Xiao, Y., Fu, L. W., Liu, M., Peng, J. Y., Improvement of
44
45
46 Thermoelectric Properties of In_4Se_3 Bulk Materials with Cu Nanoinclusions, *J. Am. Ceram. Soc.*,
47
48
49 2013, **96**, 2703.
50
51
52
53
54
55
56
57
58
59
60

1
2
3
4
5 (24) J. Y., Luo, Yang, J. Y., Li, G., Liu, M., Xiao, Y., Fu, L. W., Li, W. X., Zhu, P. W., Peng, J.
6
7
8
9
10
11
12
13
14
15
16
17
18
19
20
21
22
23
24
25
26
27
28
29
30
31
32
33
34
35
36
37
38
39
40
41
42
43
44
45
46
47
48
49
50
51
52
53
54
55
56
57
58
59
60

Y, Gao, S., Zhang, J. Q., Enhancement of the Thermoelectric Performance of Polycrystalline
In₄Se_{2.5} by Copper Intercalation and Bromine Substitution, *Adv. Energy Mater.* 2014, **4**,
1300599.

(25) Lee, M. H., Rhyee, J. S., Vaseem, M., Hahn, Y. B., Park, S. D., Kim, H. J., Kim, S. J., Lee,
H. J., Kim, C., Thermoelectric properties of SrTiO₃ nano-particles dispersed indium selenide bulk
composites, *Appl. Phys. Lett.*, 2013, **102**, 223901.

(26) Zhai, Y. B., Zhang, Q. S., Jiang, J., Zhang, T., Xiao, Y. K., Yang, S. H., Xu, G. J.,
Thermoelectric performance of the ordered In₄Se₃–In composite constructed by monotectic
solidification, *J. Mater. Chem. A*, 2013, **1**, 8844-8847.

(27) Rawat, P. K., Park, H., Hwang, J., Kim, W., Low Thermal Conductivity and High
Thermoelectric Performance in In₄Se_{3-x} with Phase-Separated Indium Inclusions, *J. Elec. Mater.*
2017, **46**, 1444-1450.

1
2
3
4
5 (28) Zhu, G.H., Lan, Y.C., Wang, H., Joshi, G., Hao, Q., Chen, G., Ren, Z.F. , Effect of selenium
6
7
8 deficiency on the thermoelectric properties of n-type $\text{In}_4\text{Se}_{3-x}$ compounds, *Phys. Rev. B*, 2011,
9
10
11 83, 115201.
12
13
14
15
16
17 (29) Ahn, K., Cho, E., Rhyee, J. S., Kim, S. II., Hwang, S., Kim, H-S., Lee, S. M., Lee, K. H.,
18
19
20 Improvement in the thermoelectric performance of the crystals of halogen-substituted
21
22
23
24 $\text{In}_4\text{Se}_{3-x}\text{H}_{0.03}$ (H = F, Cl, Br, I): Effect of halogen-substitution on the thermoelectric properties in
25
26
27 $\text{In}_4\text{Se}_{3-x}$ *J. Mater. Chem.*, 2012, **22**, 5730-5736.
28
29
30
31
32 (30) Kim, J. H., Kim, M. J., Oh, S., Rhyee, J-S., Thermoelectric properties of Se-deficient and
33
34
35 Pb-/Sn-codoped $\text{In}_4\text{Pb}_{0.01}\text{Sn}_{0.03}\text{Se}_{3-x}$ polycrystalline compounds, *J. Alloy. Compd.*, 2014, **615**,
36
37
38 933–936.
39
40
41
42 (31) Abharia, A. S., Abdellahib, M., Bahmanpour, M., The effects of Sn-substitution on
43
44
45
46 thermoelectric properties of $\text{In}_{4-x}\text{Sn}_x\text{Se}_3$ ceramic, *Ceram. Int.*, 2016, **42**, 5593–5599.
47
48
49
50
51
52
53
54
55
56
57
58
59
60

1
2
3
4
5 (32) Luu, S. D. N., Parashchuk, T., Kosonowski, A., Phan, T. B., Wojciechowski, K. T.,
6
7
8
9 Structural and Thermoelectric Properties of Solid–Liquid In_4Se_3 -In Composite, *J. Elec. Mater.*
10
11 2019, **48**, 5418–5427.
12
13
14
15
16
17 (33) Osters, O., Blazek, G., Nilges, T., Comments on Peierls-distorted Indium Chains in $\text{In}_4\text{Se}_{3-x}$,
18
19
20 *Z. Anorg. Allg. Chem.* 2013, **639**, 497–501.
21
22
23
24
25 (34) Jia, T., Chen, G., Zhang, Y., Lattice thermal conductivity evaluated using elastic
26
27 properties, *Phys. Rev. B*, 2017, **95**, 155206.
28
29
30
31
32
33 (35) Ji, H. S., Kim, H., Lee, C., Rhyee, J-S., Kim, M. H., Kaviany, M., Shim, J. H., Vacancy-
34
35 suppressed lattice conductivity of high-ZT $\text{In}_4\text{Se}_{3-x}$, *Phys. Rev. B*, 2013, **87**, 125111.
36
37
38
39
40
41 (36) Kuryachii, V. Y., Bogachev, V. Y., Mikhal'chenko, V. P., Stakhira, I. M., Elastic properties
42
43 of In_4Se_3 , *Izv. Akad. Nauk SSSR, Neorg. Mater.* 1986, **18**, 756-757.
44
45
46
47
48 (37) Zevalkink, A.; Smiadak, D. M.; Blackburn, J. L.; Ferguson, A. J.; Chabiny, M. L.; Delaire,
49
50
51 O.; Wang, J.; Kovnir, K.; Martin, J.; Schelhas, L. T.; Sparks, T. D.; Kang, S. D.; Dylla, M. T.;
52
53
54
55
56
57
58
59
60

1
2
3
4
5 Snyder, G. J.; Ortiz, B. R.; Toberer, E. S. A practical field guide to thermoelectrics:
6
7
8 Fundamentals, synthesis, and
9
10
11
12 characterization, *App. Phys. Rev.* 2018, **5**, 021303.
13
14

15
16 (38) Asmani, M., Kermel, C., Leriche, A., Ourak, M., Influence of porosity on Young's modulus
17
18 and Poisson's ratio in alumina ceramics, *J. Eur. Ceram. Soc.*, 2001, **21**, 1081-1086.
19
20
21
22

23
24 (39) Anderson, O. L., A simplified method for calculating the Debye temperature from elastic
25
26 constants, *J. Phys. Chem. Solids*, 1963, **24**, 909-917.
27
28
29
30

31
32 (40) Kurosaki, K., Kosuga, A., Muta, H., Uno, M., Yamanaka, S., Ag_9TiTe_5 : A high-performance
33
34 thermoelectric bulk material with extremely low thermal conductivity, *Appl. Phys. Lett.*, 2005, **87**,
35
36 061919.
37
38
39
40
41

42
43 (41) Sanditov, D. S., Belomestnykh, V. N., Relation between the parameters of the elasticity
44
45 theory and averaged bulk modulus of solids, *Tech. Phys.* 2011, **56**, 1619-1623.
46
47
48
49
50
51
52
53
54
55
56
57
58
59
60

1
2
3
4
5 (42) Belomestnykh, V.N., Tesleva, E.P., Interrelation between anharmonicity and lateral strain
6
7
8

9 in quasi-isotropic polycrystalline solids, *Tech. Phys.* 2004, **49**, 1098-1100.
10
11
12

13 (43) Kim, H.-S.; Gibbs, Z. M.; Tang, Y.; Wang, H.; Snyder, G. J. *APL Materials*, 2015, **3**,
14
15
16 041506.
17
18
19
20

21 (44) Slack, G., Nonmetallic crystals with high thermal conductivity, *J. Phys. Chem. Solids*,
22
23
24 1973, **34**, 321-335.
25
26
27
28
29

30 (45) Cahill, D. G., Watson, S. K., Pohl, R. O., Lower limit to the thermal conductivity of
31
32 disordered crystals, *Phys. Rev. B* 1992, **46**, 6131-6140
33
34
35
36

37 (46) Giannozzi, P., Baroni, S., Bonini, N., Calandra, M., Car, R., Cavazzoni, C., Ceresoli, D.,
38
39 Chiarotti, G. L., Cococcioni, M., Dabo, I., Corso, A. Dal., Gironcoli, S. de, Fabris, S., Fratesi, G.,
40
41 Gebauer, R., Gerstmann, U., Gougaussis, C., Kokalj, A., Lazzeri, M., Martin-Samos, L., Marzari,
42
43 N., Mauri, F., Mazzarello, R., Paolini, S., Pasquarello, A., Paulatto, L., Sbraccia, C., Scandolo,
44
45
46 N., Sclauzero, G., Seitsonen, A. P., Smogunov, A., Umari, P., Wentzcovitch, R. M., QUANTUM
47
48
49
50
51
52
53
54
55
56
57
58
59
60

1
2
3
4
5 ESPRESSO: a modular and open-source software project for quantum simulations of materials,
6
7
8

9 *J. Phys.: Condens. Matter*, 2009, **21**, 395502
10
11
12

13 (47) Supka, A. R., Lyons, T. E., Liyanage, L., D'Amico, P., Al Rahal Al Orabi, R., Mahatara, S.,
14
15

16 Gopal, P., Toher, C., Ceresoli, D., Calzolari, A., Curtarolo, S., Nardelli, M. B., Fornari, M.,
17
18

19 AFLOW π : A minimalist approach to high-throughput ab initio calculations including the
20
21

22 generation of tight-binding hamiltonians, *Comput. Mater. Sci.*, 2017, **136**, 76-84.
23
24

25 (48) Setten, M. J. V., Giantomassi, M., Bousquet, E., Verstraete, M. J., Hamann, D. R., Gonze,
26
27

28 X., Rignanese, G.-M., The PseudoDojo: Training and grading a 85 element optimized norm-
29
30

31 conserving pseudopotential table, *Comput. Phys. Commun.*, 2018, **226**, 39-54.
32
33

34 (49) Nardelli, M. B., Cerasoli, F. T., Costa, M., Curtarolo, S., De Gennaro, R., Fornari, M.,
35
36

37 Liyanage, L., Supka, A. R., Wang, H., PAOFLOW: A utility to construct and operate on ab initio
38
39

40 Hamiltonians from the projections of electronic wavefunctions on atomic orbital bases, including
41
42

43 characterization of topological materials, *Comp. Mat. Sci.* 2018, **143**, 462-472
44
45

1
2
3
4
5 (50) Golesorkhtabar, R., Pavone, P., Spitaler, J., Puschnig, P., Draxl, C., ElaStic: A tool for
6
7
8 calculating second-order elastic constants from first principles, *Comput. Phys. Commun.*, 2013,
9
10
11 184, 1861–1873
12
13
14
15
16
17 (51) Zhang, Y., First-principles Debye–Callaway approach to lattice thermal conductivity, *J.
18
19
20 Materiomics*, 2016, 2, 237-247
21
22
23
24
25 (52) Hogg, J. H. C., Sutherland, H. H., Williams, D. J., The crystal structure of tetraindium
26
27 triselenide, *Acta Crystallogr. B*, 1973, B29, 1590-1593
28
29
30
31
32 (53) Wolcyrz, M., Kubiak, R., Maciejewski, S., X-ray investigation of thermal expansion and
33
34 atomic thermal vibrations of tin, indium, and their alloys, *Phys. Status Solidi B*, 1981, 107, 245-
35
36
37
38
39 253
40
41
42
43
44 (54) Cordero, B., Gómez, V., Platero-Prats, A. E., Revés, M., J. Echeverría, E. Cremades,
45
46
47 F.Barragán, S. Alvarez, Covalent radii revisited, *Dalton Trans.*, 2008, 21, 2832–2838
48
49
50
51
52
53
54
55
56
57
58
59
60

1
2
3
4
5 (55) Jones, R. E., Templeton, D. H., The crystal structure of indium (I) iodide, *Acta Crystallogr.*
6

7
8 1955, **8**, 847
9

10
11
12 (56) Shannon, R. D., Revised effective ionic radii and systematic studies of interatomic
13
14 distances in halides and chalcogenides, *Acta Crystallogr A*. 1976, **A32**: 751–767
15
16

17
18
19 (57) Losovyj, Y. B., Makinistian, L., Albanesi, E. A., Petukhov, A. G., Liu, J., Galiy, P., Dveriy,
20
21 O. R., Dowben, P. A., The anisotropic band structure of layered In₄Se₃(001), *J. Appl. Phys.*,
22
23
24 2008, **104**, 083713.
25
26
27

28
29
30
31 (58) Walsh, A., Payne, D. J., Egddell, R. G., Watson, G. W., Stereochemistry of post-transition
32
33 metal oxides: revision of the classical lone pair model, *Chem. Soc. Rev.*, 2011, **40**, 4455–4463
34
35

36
37
38
39 (59) Hanus, R., Agne, M. T., Rettie, A. J. E., Chen, Z., Tan, G., Chung, D. Y., Kanatzidis, M.G.,
40
41
42 Pei, Y., Voorhees, P. W., Snyder, G. J., Lattice Softening Significantly Reduces Thermal
43
44
45 Conductivity and Leads to High Thermoelectric Efficiency, *Adv. Mater.* 2019, **31**, 1900108
46
47
48
49
50
51
52
53
54
55
56
57
58
59
60

1
2
3
4
5 (60) Kallel, A.C., Roux, G., Martin, C.L., Thermoelectric and mechanical properties of a hot
6
7
8
9 pressed nanostructured n-type $\text{Si}_{80}\text{Ge}_{20}$ alloy, *Mater. Sci. Eng. A.*, 2013, **564**, 65-70
10
11
12
13 (61) Schmidt, R., Fan, X., Case, E., Sarac, P., Mechanical properties of Mg_2Si thermoelectric
14
15
16 materials with the addition of 0–4 vol% silicon carbide nanoparticles (SiCNP), *J. Mater. Sci.*,
17
18
19 2015, **50**, 11, 4034-4046
20
21
22
23
24 (62) Ni, E. J., Casea, D.E., Khabir, N.K., Stewart, C.R., Wub, Ch-I., Hoganb, P.T., Timmc, J.
25
26
27 E., Girardd, N.S., Kanatzidis, G. M., Room temperature Young's modulus, shear modulus,
28
29
30 Poisson's ratio and hardness of PbTe–PbS thermoelectric materials, *Mat. Sci. Eng. B*, 2010,
31
32
33 170, 58–66
34
35
36
37
38 (63) Li, M. Kazi Nazrul Islam, Md. Sh., Yahyaoglu,M., Pan,D., Shi,X., Chen, L.D., Aydemir. U.,
39
40
41 Wang, X., Ultrahigh figure-of-merit of Cu_2Se incorporated with carbon coated boron
42
43
44 nanoparticles, *InfoMat*. 2019;1:108–115
45
46
47
48
49
50
51
52
53
54
55
56
57
58
59
60

1
2
3
4
5 (64) Ashby, M. F., Materials Selection in Mechanical Design, 4th Edi. Butterworth Heinemann,
6
7
8
9 2011
10
11
12

13 (65) Lin, S., Li, W., Li, S., Zhang, X., Chen, Z., Xu, Y., Chen, Y., Pei, Y., High Thermoelectric
14
15
16 Performance of Ag_9GaSe_6 Enabled by Low Cut off Frequency of Acoustic Phonons, *Joule*, 2017,
17
18
19 1, 816-830
20
21
22
23

24 (66) Toberer, E.S., Zévalkink, A., Snyder, G.J., Phonon engineering through crystal chemistry, *J. Mater.*
25
26 *Chem.*, 2011, **21**, 15843-15852
27
28
29

30 (67) Vaqueiro, P., Al Orabi, R. A. R., Luu, S. D. N., Guélou, G., Powell, A. V., Smith, R. I.,
31
32 Song, J.-P., Wee, D., Fornari, M., The Role of Copper in The Thermal Conductivity of
33
34 Thermoelectric Oxychalcogenides: Do Lone Pairs Matter?, *Phys. Chem. Chem. Phys.* 2015, **17**,
35
36
37 31735- 31740.
38
39
40
41
42
43
44

45 (68) Plata, J. J., Nath, P., Usanmaz, D., Carrete, J., Toher, C., Jong, M. D., Asta, M. D., Fornari,
46
47 M., Nardelli, M. B., Curtarolo, S., An efficient and accurate framework for calculating lattice
48
49
50
51
52
53
54
55
56
57
58
59
60

1
2
3
4
5 thermal conductivity of solids: AAPL - AFLOW Anharmonic Automatic Phonon Library, *NPJ*
6
7
8
9 *Comp. Mat.* 2017, **3**, 45 .
10
11
12
13 (69) Bourgs, C., Bouyrie, Y., Supka, A., Al Orabi, R. A. R., Lemoine, P., Lebedev, O., Ohta, M.,
14
15
16 Suekuni, K., Nassif, V., Hardy, V., Daou, R., Miyazaki, Y., Fornari, M., Guilmeau, E., High-
17
18
19 performance Thermoelectric Bulk Colusite by Process Controlled Structural Disorder, *J. Am.*
20
21
22
23
24 *Chem. Soc.* 2018, **140**, 2186-2195 .
25
26
27
28 (70) Nielsen, M. D., Ozolins, V., Heremans, J. P., Lone pair electrons minimise lattice thermal
29
30
31 conductivity, *Energy Environ. Sci.* 2013, **6**, 570-578.
32
33
34
35
36
37
38
39
40
41
42
43
44
45
46
47
48
49
50
51
52
53
54
55
56
57
58
59
60

